THERMOHALINE CONVECTION AT A SHARP DENSITY INTERFACE

Hosoyamada, Tokuzo
Department of Civil Engineering Hydraulics and Soil Mechanics, Kyushu University : Postgr., Dep

Honji, Hiroyuki
Research Institute for Applied Mechanics, Kyushu University : Professor

https://doi.org/10.5109/6781096

出版情報：Reports of Research Institute for Applied Mechanics. 36 (106), pp.1-13, 1989-09. 九州大学応用力学研究所
バージョン：
権利関係：

Reports of Research Institute for Applied Mechanics
Vol. XXXVI, No. 106, 1989

THERMOHALINE CONVECTION AT A SHARP DENSITY INTERFACE

By Tokuzo HOSOYAMADA* and Hiroyuki HONJI**

Two types of thermohaline convective flows have been investigated experimentally using a double diffusion tank with a horizontally-removable plate: The first type concerns salt-finger convection and the second type heat-driven one. An initial growth rate of the embryos of salt fingers has been measured based on a flow visualization. A set of time series of the temperature fluctuation due to the two types of convection have also been measured with a thermocouple system. A cumulative correlation dimension for the salt finger type is 1.49 and that for the heat-driven one, basically similar to Bénard convection, is 1.50. This approximate equivalence suggests that the salt-finger convection may have a chaotic-dynamical similarity to Bénard convection.

Key words: Salt finger, Double diffusion, Fractal dimension

1. Introduction

Convection in fluids plays a basic role in the mixing and diffusion processes of scalar quantities in the ocean environment. Both thermal and double-diffusive, thermohaline, convective phenomena have long been investigated in this connection. In particular, Bénard convection has been a subject of many investigations. As far as thermohaline convection is concerned, however, much remains to be settled before it is fully understood. Moreover, a new approach exemplified by such concepts as chaos and fractals to convective flows has been opened up recently, and again there is need for a fresh look at thermohaline convection[1,2].

* Postgr., Dept. Civil Eng. Hydr. & Soil Mech., Kyushu Univ., Fukuoka 812, Jpn.
** Prof., Res. Inst. Appl. Mech., Kyushu Univ., Kasuga 816, Jpn.

The problem of double-diffusive instability has been investigated often by using salt and sugar as two diffusive components, because of the easiness of controlling sugar instead of heat[3]. However, a salt-sugar system is not dynamically similar to the heat-salt one[4]. It is, therefore, desirable to investigate the instability driven directly by salinity and temperature differences.

The above consideration has led us to develop a new type of apparatus for setting up a thermohaline (heat-salt) system[5]. The system enables us to form a "sharp" interface with a step-wise distribution of salinity and temperature. Two types of the distribution of salinity and temperature have been considered in connection with double diffusive instabilities[4]. One is the distribution related to salt-finger convection; the upper layer has an excess of the heat and solute but still less dense than the lower one. Another is that related to heat-driven convection; the lower layer has an excess of the heat and solute. These two experimental configurations can be set up easily with the new apparatus.

This paper reports some laboratory results related to the above two types of convection, which is induced at a relatively sharp interface of salinity and temperature distribution in the diffusion tank.

2. Experimental methods

Experiments were carried out using a rectangular water tank made of transparent Perspex plates with the thickness of 1.5 cm. The dimension of the tank is $80 \times 40 \times 40$ cm as shown in Fig. 1. The tank is equipped with a horizontally removable plate: Further details of the tank is described in ref. 5. The working fluids were separated initially into the upper and lower parts by the plate. For the salt-finger convection, the water in upper room 1 was kept salty and warm, and that in lower room 2 fresh and cold. For the heat-driven convection, the water in upper room 1 was kept fresh and cold, and that in lower room 2 salty and warm. Each water mass had been circulated separately until

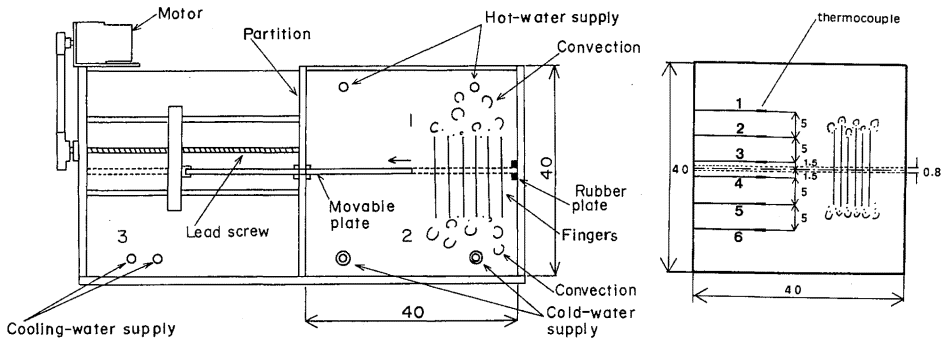

Fig. 1 Side view of experimental apparatus (Dimension in cm)

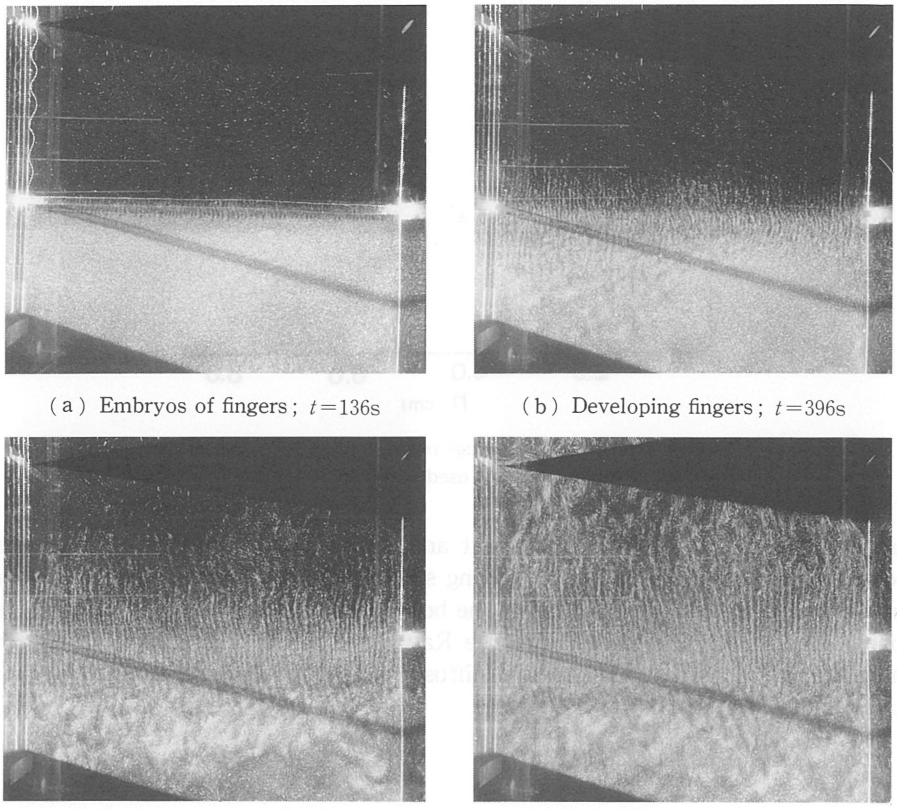

(a) Embryos of fingers; $t=136$s (b) Developing fingers; $t=396$s

(c) Developing fingers; $t=985$s (d) Fully developed fingers; $t=1528$s

Fig. 2 Flow patterns of salt fingers (Side views):
$R_a=1.06\times10^{10}$, $R_s=8.36\times10^{8}$, $\tau=9.58\times10^{-3}$, $P_r=7.27$

a desired difference of its temperature was reached. Then, the horizontal plate was removed into room 3 slowly. As the waters in rooms 1 and 2 met behind the edge of the plate, salt fingers began to grow at the interface having the same level as the removed plate.

The aluminum powder method was used for flow visualization; a vertical or horizontal sheet of the water was illuminated from side for photography with a 1kW slide projector. Flow patterns were photographed consecutively from side and from above of the tank with a 35 mm camera. Water temperature was measured with six thermocouples aligned in a vertical plane as shown in Fig. 1.

3. Results and Discussion

3.1. Salt fingers

Salt fingers form at the interface between upper and lower layers: the

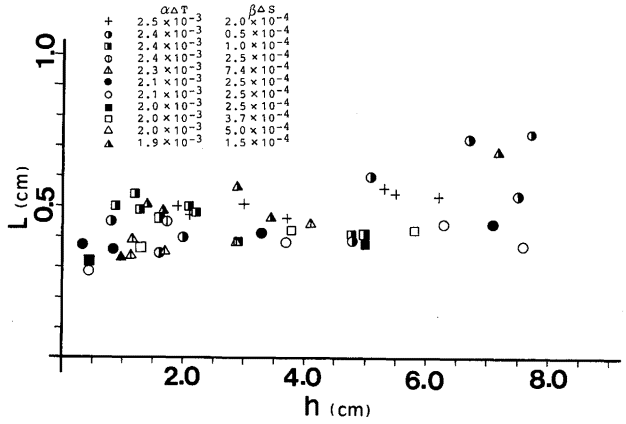

Fig. 3 Horizontal wave length (spacing) of fingers plotted against vertical finger length (The same symbols are used in Figs. 3 to 5)

upper layer has an excess of the heat and solute but still less dense than the lower layer. An example of developing salt fingers is shown in Fig. 2, where t is the time which has elapsed after the beginning of removal of the plate. The parameters R_a, R_s, τ, and P_r are the Rayleigh number, the salinity Rayleigh number, the ratio of salinity to heat diffusivity, and the Prandtl number, respectively: they are defined as follows

$$R_a = \frac{g\alpha \Delta T}{k_T \nu} d^3 ,$$

$$R_s = \frac{g\beta \Delta S}{k_T \nu} d^3 ,$$

$$\tau = \frac{k_s}{k_T} , \quad \text{and}$$

$$P_r = \frac{\nu}{k_T} ,$$

where ΔT and ΔS are the initial temperature and salinity differences at $t=0s$, respectively. The parameters α, β, ν, k_t, and k_s are the temperature and salinity expansion coefficients, the kinematic viscosity, the thermal and salinity diffusion coefficients in water, respectively. These five parameters are calculated as a function of representative temperature and salinity, which are the average temperature and salinity of the upper and lower fluids. The parameters g and d are the acceleration due to gravity and a representative vertical scale of convection. Throughout d is taken as 40 cm, the depth of the tank.

Figure 2(a) shows a side view of the embryos of salt fingers formed while the plate is still moving to the left. The upper and lower water layers still remain

almost undisturbed. Figures 2(b) and (c) show the growing salt fingers togethcer with the large scale convections induced above and below the layer of salt fingers. Figure 2 (d) shows a cross-sectional view of fully developed salt fingers. The top of the salt fingers becomes unstable. The vertical exchange of the upper and lower fluids due to a local unstable density distribution drives the salt fingers and the large-scale vertical convections. The fingering motion and convection dissipate due to the vertical transport of heat and solute by thce vertical exchange of the waters.

Figure 3 shows the h dependence of L, where h is the finger height, L the horizontal wave length (spacing) of salt fingers. Experimental conditions are indicated by the values of $\alpha\Delta T$ and $\beta\Delta S$, the non-dimensional density anomaly due to the temperature distribution and the salinity distribution, respectively. The value of L increases slightly with increasing h. According to the linear stability theory[4], the horizontal wave number corresponding to the maximum growth rate is given by

$$L_{\max} = \left\{\frac{g}{k_T\nu}(\alpha\bar{T}_z - \beta\bar{S}_z)\right\}^{-\frac{1}{4}} \text{[4]},$$

where $\bar{T}_z$ is an average temperature gradient and $\bar{S}_z$ an average salinity gradient. In this experiment associated with a sharp interface of temperature and salinity distribution, the values of $\bar{T}_z$ and $\bar{S}_z$ are represented by $\Delta T/d$ and $\Delta S/d$, respectively. The above result seems to be valid only initially, i. e. immediately after the meeting of the upper and lower waters.

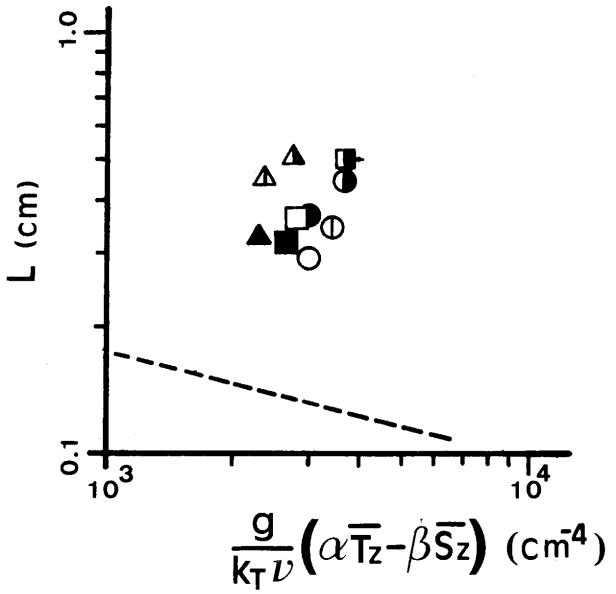

Fig. 4 Comparison of L with linear stability theory indicated by dashed line

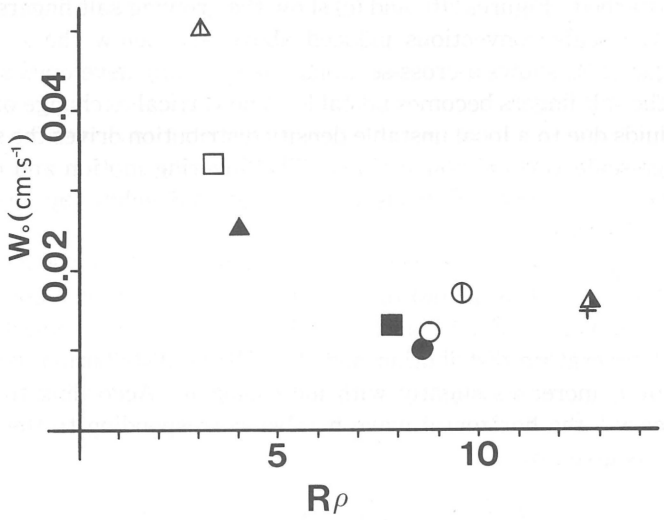

Fig. 5 Variation of initial growth rate (W_o) of salt fingers

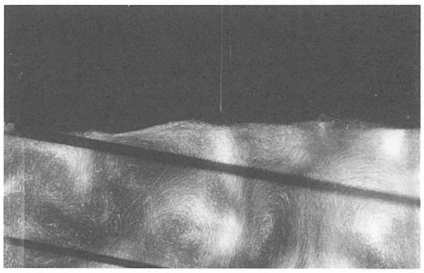

Fig. 6 Stable interface disturbed by convection (Side view): $R_a=9.40\times10^8$, $R_s=9.27\times10^8$, $\tau=8.60\times10^{-3}$, $P_r=8.6$

Figure 4 shows the plot of L for the fingers at their first appearance to the naked eyes, against the values for the quantity in the curley brackets in the above equation. The broken line is drawn based on the linear stability theory. As will be seen from the figure, there is a discrepancy between experimental and theoretical values. This may perhaps be due to the fact that the visualized embryos of fingers are already beyond the range to be described by the linear theory. Figure 5 shows the relationship between W_o, the rate of finger growth in height at earlier stages, and $R_\rho=\alpha\Delta T/\beta\Delta S$. The decrease of the value of R_ρ promotes the exchange of the upper and lower waters and also the growth of the salt-fingers, because the heat makes the upper water lighter and the salinity makes it heavier. The value of W_o decreases as R_ρ increases.

3.2. Heat-driven convection

When the lower layer of water has an excess of the heat and solute and is more dense than the upper layer, the interface between the two layers is destabilized with the convection induced in each layer separately. The convection of the lower layer is driven by cooling from the upper layer, and the convection of the upper layer is driven by heating from the lower layer. Figure 6 shows a disturbed sharp interface under which convective eddies are seen : the aluminum powder was suspended only in the lower layer. The stable density

Fig. 7 Temporal development of unstable interface at $t<30$s (side view) : $R_a=1.19\times10^9$, $R_s=8.98\times10^8$, $\tau=8.36\times10^{-3}$, $P_r=8.7$

distribution prevented the upper and lower fluids from mixing. Although the interface was tossed up and down by the convection in each layer, it remained quite sharp.

An unstable interface which develops into vigorous convection is shown in a series of photographs in Fig. 7. The interface becomes unstable only when the lower water is less dense than the upper one. The unstable convective motion near the interface was amplified quickly and the upper and lower waters were overturned and mixed well. There is a considerable difference between the salt-finger convection and the heat-driven convection in the development of instability. In the former case, the stable interface always becomes unstable after the upper and lower waters meet. In the latter case, if the interface is stable when the both waters meet, the interface remains sharp and stable. If the lower layer is less dense than the upper layer and the interface is unstable, a vigorous convective motion is established in the whole water.

3.3. Fluctuation of water temperatures

Figure 8 shows a time series of the output voltage from the thermocouples in the case of the salt-finger type convection. The fluctuation of the output voltage is considered as showing that of water temperature, because the output voltage is converted to temperature almost linearly. The broken line indicates the time at which the edge of the horizontal plate passes through the vertical cross section including the aligned thermocouples. Immediately after the upper

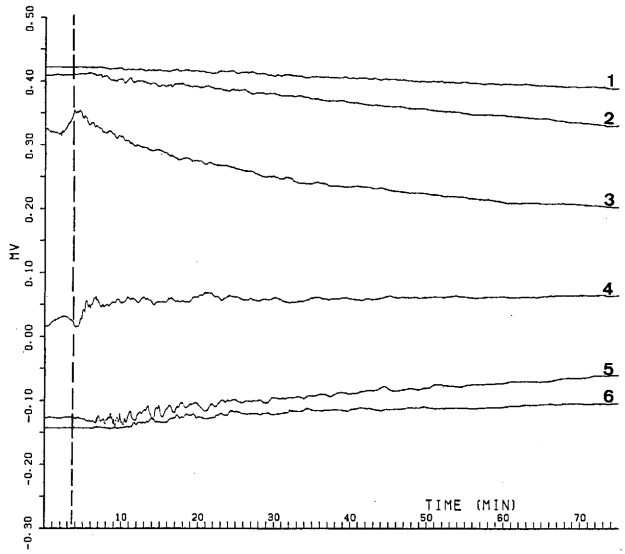

Fig. 8 Output voltage from thermocouple (Salt fingers)
$R_a=11.1\times10^9$, $R_s=2.06\times10^9$, $\tau=9.51\times10^{-3}$, $P_r=7.34$

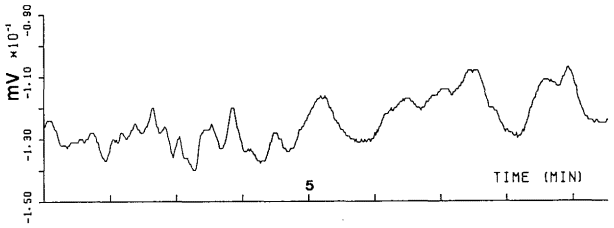

Fig. 9 Fluctuation of output voltage from thermocouple (Salt fingers)

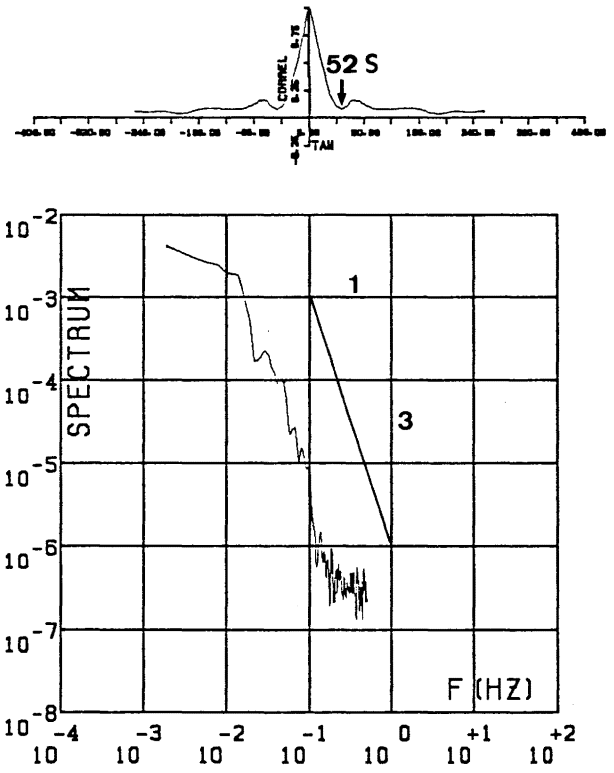

Fig. 10 Auto-correlation coefficient (upper figure) and power spectrum (ordinate in $mV^2 \cdot s$) (Salt fingers)

and lower waters meet, the output voltage from the thermocouples (2) and (3) (in Fig. 1) which are set near the center of the interface are fluctuating due to the meeting of the lower and upper waters. The fluctuation of the output voltage from the thermocouple (5) (Fig. 1) located near the lower end of the finger region is most conspicuous at $t=7$ to 18 min.

Figure 9 shows a fluctuating portion of the above time series. In the

analysis, the mean component was assumed to vary linearly with time and subtracted from the original data. Figure 10 shows the auto-correlation coefficient and the power spectrum for the fluctuating component shown in Fig. 9. The FFT method was used to obtain the power spectrum ; the number of the data was 512. The power spectrum decreases approximately in proportion to the power of -3 of the frequency. The auto-correlation coefficient has the minimum value at 52s, which is the characteristic time for the time series to lose the correlation. Recently, a truncated system of equations concerning double-diffusive convection has been developed, and the chaotic solutions have been found for the system[1,2].

Information on the chaotic behavior of the system can also be derived from the cumulative correlation functions and the cumulative correlation dimensions associated with the fluctuation data of laboratory experiments. A cumulative correlation function $C(r)$ is[6]

$$C(r) = \frac{1}{N^2} \sum_{k,j=1}^{N} H(r - |\boldsymbol{x}_k - \boldsymbol{x}_j|) \ ,$$

where N and H are the number of the data and the Heaviside function, respectively. In the above equation, r is a kind of "radius" which is defined on p. 217 of ref. 6. A vector $\boldsymbol{x}$ obtained from the time series $x(t)$ is

$$\boldsymbol{x}_i = (x(t_i), x(t_i + t'), \ldots, x(t_i + (m-1)t')) \ ,$$

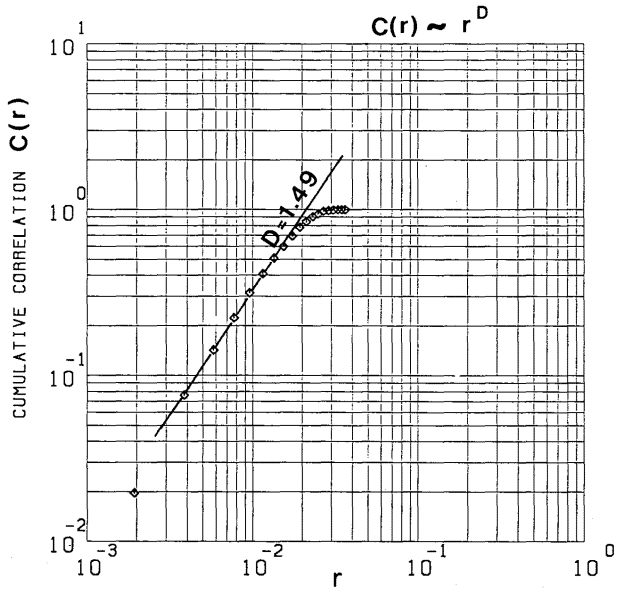

Fig. 11 Plot of cumulative correlation function as a function of distance between selected vectors (Salt fingers)

where t' is the characteristic time determined from the auto-correlation coefficient: $t'=52$s which appeared before. The value of m selected to maximize the cumulative correlation dimension which will be defined later is 2. It should be noted that the same correlation dimension has been obtained for $m=2$ and $m=3$. The norm on the attractor $|\boldsymbol{x}_k-\boldsymbol{x}_j|$ is obtained from the time series data. A determination of the correlation dimension is made by plotting $C(r)$ against r on a log-log graph. The region in which the power law obeyed appears

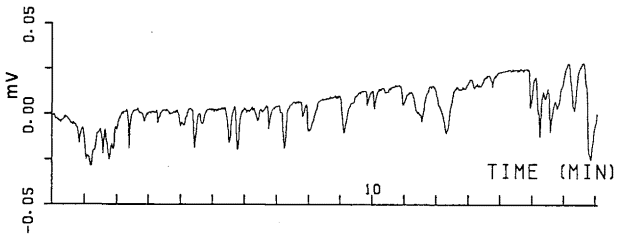

Fig. 12 Fluctuation of output voltage from thermocouple (Heat driven-convection)

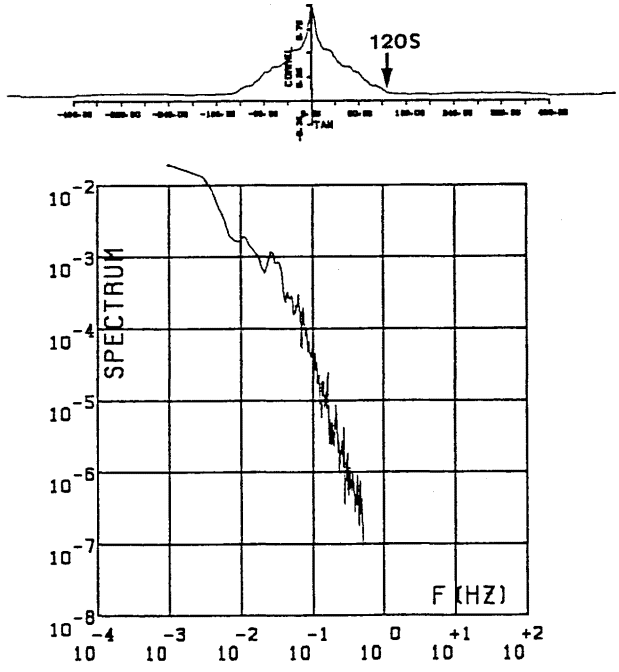

Fig. 13 Auto-correlation coefficient (upper figure) and power spectrum (ordinate in $mV^2 \cdot s$) (Heat-driven convection)

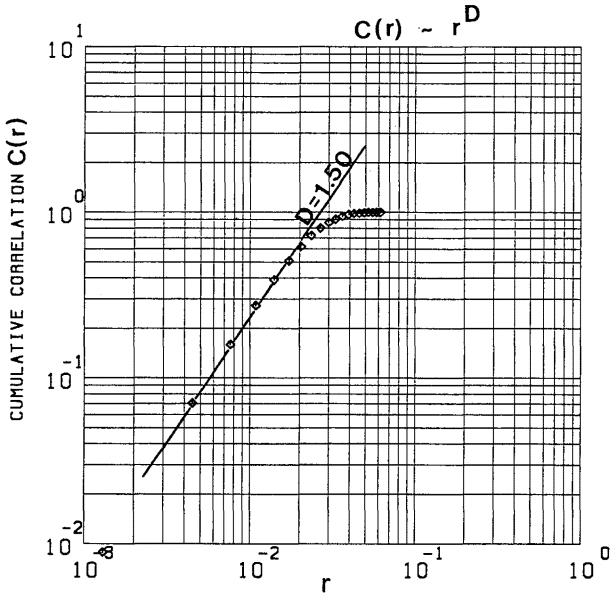

Fig. 14 Plot of cumulative correlation function as a function of distance between selected vectors (heat-driven convection)

as a straight line; the slope is defined as the cumulative correlation function. Figure 11 shows the plot of $C(r)$ against r, where the cumulative correlation exponent is 1.49.

The same procedure has been applied to a case of the heat-driven convection which maintains a stable interface. The fluctuation of the temperature just above the interface is shown in Fig. 12. Figure 13 shows the auto-correlation coefficient and power spectrum of the fluctuation for the case shown in Fig. 12. Figure 14 shows the plot of $C(r)$ against r on a log-log graph, where the cumulative correlation dimension is 1.50. The cumulative correlation dimension for the salt finger convection and that for the stable heat driven convection are almost the same non-integer value. This approximate equivalence of the fractal dimension suggests that the two types of convection are of the same origin: The whole pattern of fingers as a group looks different from that of Bénard convection, but both patterns look similar in a localized scale. This means that the salt-finger convection may have a chaotic-dynamical similarity to Bénard convection.

Acknowledgment

This work was supported by a Ministry of Education grant for the Priority Area Research Programme 'Dynamics of the Deep Ocean Circulation', which is

gratefully acknowledged.

References

1) Knobloch, E., Moore, D. R., Toomre, J. and Weiss, N. O.: Transition to chaos in two-dimensional double-diffusive convection, J. Fluid Mech. **106** (1986) 409-448.
2) Yanase, S.: Chaos in double-diffusive convection, J. Jpn. Soc. Fluid Mech. **7** (1987) 3-14.
3) Shirtcliff, T. G. L. and Turner, J. S.: Observation of cell structure of salt fingers, J. Fluid Mech. **7** (1969) 707-719.
4) Stern, E.: Ocean Circulation Physics, Academic Press, 1975, N, Y., pp. 189-215.
5) Hosoyamada, T. and Honji, H.: A thermohaline-diffusion tank with a movable plate, Exper. in Fludis **7** (1989), 208-210.
6) Henderson, H. W. and Wells, R.: Obtaining attractor dimensions from meteorological time series, Advances in Geophysics **30** (1988), Academic Press, N. Y., pp. 205-237.
7) Weiss, N. O.: Dynamics of convection, Proc. R. Soc. Lond. **A413** (1987), 71-85.

(Received June 30, 1989)